EPJ D
Atomic, Molecular, Optical and Plasma Physics
EPJ.org
your physics journal

Eur. Phys. J. D **59**, 43–51 (2010) DOI: 10.1140/epjd/e2010-00084-9

Control and managing of localized states in two-dimensional systems with periodic forcing

M.G. Clerc, F. Haudin, S. Residori, U. Bortolozzo and R.G. Rojas

EDP SCIENCES
Società Italiana di Fisica
Springer

Eur. Phys. J. D **59**, 43–51 (2010)
DOI: 10.1140/epjd/e2010-00084-9

THE EUROPEAN PHYSICAL JOURNAL D

Regular Article

Control and managing of localized states in two-dimensional systems with periodic forcing

M.G. Clerc[1,a], F. Haudin[2], S. Residori[2], U. Bortolozzo[2], and R.G. Rojas[3]

[1] Departamento de Física, FCFM, Universidad de Chile, Casilla 487-3, Santiago, Chile
[2] INLN, Université de Nice Sophia-Antipolis, CNRS, 1361 route des Lucioles, 06560 Valbonne, France
[3] Instituto de Física, Pontificia Universidad Católica de Valparaíso, Casilla 4059, Valparaíso, Chile

Received 10 December 2009 / Received in final form 6 February 2010
Published online 30 March 2010 –

Abstract. We study the formation of localized structures in two-dimensional systems with periodic forcing, showing that these types of systems provide an adequate framework for the study and control of localized structures. Theoretically, we introduce a dissipative ϕ^4 model as a prototype for a bistable spatially forced system, and we show that with different spatial forcings of small amplitudes, such as square or hexagonal grids, this model exhibits a family of localized structures. By changing the forcing parameters, we control the bistability between the various induced patterns. Experimentally, based on an optical feedback with spatially amplitude-modulated beam, we set-up a two-dimensional forced experiment in a nematic liquid crystal cell. By changing the forcing parameters, the system exhibits a family of localized structures that are confirmed by numerical simulations for the average liquid crystal tilt angle.

1 Introduction

Non-equilibrium systems often exhibit different stationary states for different initial conditions. Multistability is, therefore, one of the typical features of this class of systems. Spatially extended multistable systems can exhibit solutions connecting two different steady states, and these types of solutions are commonly denominated fronts [1]. The concept of front propagation, emerged in the field of population dynamics [2,3], has gained growing interest in biology [4], chemistry [5,6], physics [1,7,8] and mathematics [9,10]. On the other hand, spatial patterns appear spontaneously in out-of-equilibrium systems and are observed in many different physical contexts [11]. During the last two decades, spatial pattern formation has been largely studied, leading to the identification of various types of spatio-temporal instabilities and symmetry selection processes in the general framework of dynamical systems and bifurcation theory [11]. Localized structures, that is, patterns extended over a restricted spatial domain, have received, in particular, a large interest, and from the early observations of magnetic domains in ferromagnetic materials [12], localized states have been successively observed in such different systems as liquid crystals [13], plasmas [14], chemical reactions [15], fluid surface waves [16], granular media [17,18], and thermal convection [19,20], just to cite a few. In nonlinear optics localized structures were first predicted as solitary waves in bistable optical cavities [21], and successively explained in terms of diffractive auto-solitons [22]. Optical localized structures attract nowadays a lot of interest since they are potential candidates for optical memories (see the review [23] and references therein).

All these intriguing observations have inspired many theoretical works on the origin of localized structures. Most of them are based onto a one-dimensional geometrical description, in which localized structures are understood as the homoclinic orbits in the Poincaré section of the corresponding spatial-reversible dynamical system [24–26]. In this framework, localized structures are predicted to exist in parameter regions where the system exhibits bistability between a pattern and an uniform stable state. Localized spatial states are, thus, understood as macroscopic particle-like objects realizing the spatial connection between two metastable states and appearing close to the *pinning range* of the front solution [27]. Inside the pinning range, the bifurcation diagram displays a *snaking* shape with an infinite sequence of saddle-node bifurcations, each bifurcation creating a cell of the localized pattern solution [25]. Extensions of the same scenario have been given in later papers [28–30]. More recently, localized structures have been described in terms of front interactions [31] and their existence has been generalized to the case when the homoclinic orbits connect two pattern states, thus leading to *localized peaks* [32].

The experimental verification of all the theoretical descriptions needs the bistability, either between two patterns or between a pattern and a uniform state. However,

[a] e-mail: marcel@dfi.uchile.cl

as a consequence of the slanted homoclinic snaking bifurcation diagram [33,34], localized structures can be observed even outside the bistability region. In fact, the experimental observations show that a reduced number of localized structures survive outside, and even far from, the bistability region [35]. Experimentally, the main challenge is the control of localized structures, which resorts to the ability of mastering the bistability, that is, selecting the type of metastable states, controlling the width of the bistable region and the pinning range. However, managing the bistability of self-organizing patterns is a very complex task, which also lacks theoretical supports whenever we deal with systems with more than one spatial dimension.

The aim of this manuscript is to show that bistability together with spatial forcing provide an adequate framework where to study and control localized structures. Theoretically, we introduce a prototype model for a spatially bistable forced system – a dissipative forced ϕ^4 model – with different moderate forcings, such as square or hexagonal grids, that exhibits a family of localized structures. We show that, by changing the forcing parameters, we can control the bistability between the different self-organizing patterns. Experimentally, based on an optical feedback with spatially amplitude-modulated beam, we set-up a two-dimensional forced experiment in a nematic liquid crystal cell. By changing the forcing parameters, the system exhibits a family of localized structures. The experimental findings are confirmed by numerical simulations for the average liquid crystal tilt angle.

The paper is organized as follows. Section 2 presents a phenomenological bistable model with spatial forcing and the numerically calculated localized structures that can be obtained for different forcing parameters. In Section 3 we present the experimental set-up, that is based on a liquid crystal light valve LCLV with optical feedback, and the theoretical description of the full model for the spatially forced LCLV. In Section 4 are reported the localized structures observed in the experiment under different forcing conditions. Finally, Section 5 presents the conclusions and further perspectives.

2 Theoretical description: a simple bistable model with spatial forcing

In order to have a simple model that exhibits bistability in two-dimensional spatial dynamical systems, let us introduce the dissipative ϕ^4 model

$$\partial_t u = \eta + \mu u - u^3 + \nabla_\perp^2 u, \tag{1}$$

where $u(x,t)$ is a scalar field, μ is the bifurcation parameter, η accounts for the asymmetry between the two homogeneous states and $\nabla_\perp^2 \equiv \partial_{xx} + \partial_{yy}$ is the transverse Laplacian operator. From the bifurcation viewpoint, the above model describes an extended imperfect pitchfork bifurcation [37]. The above equation can read as

$$\partial_t u = -\frac{\delta F}{\delta u}, \tag{2}$$

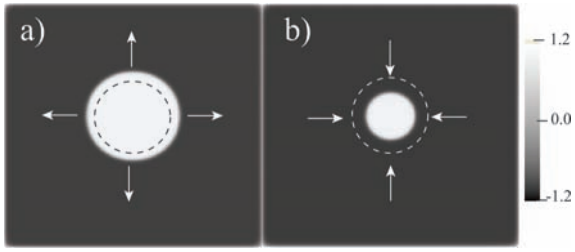

Fig. 1. Front propagation of the dissipative ϕ^4 model equation (1), by $\eta = 0.1$ and $\mu = 1$. The dashed circle represents the nucleation barrier.

where

$$F = -\int \left[\eta u + \mu u^2/2 - u^4/4 - \left(\nabla_\perp u\right)^2/2\right] dxdy \tag{3}$$

is a Lyapunov function. Hence, the dynamics of model (1) is characterized by the minimization of F. Inside the curve $\eta^2 = 2(\mu/3)^3$ in $\{\eta, \mu\}$-space, the system exhibits three uniform states, two stable and one unstable, and outside this curve there is only one stable state. Therefore, the system has a bistability region inside the $\eta^2 = 2(\mu/3)^3$ curve and undergoes a saddle-node bifurcation at the boundaries. The origin of the $\{\eta, \mu\}$-space is a point of nascent bistability [36] or a cusp point [37].

In the bistability region, the model (1) shows front solutions connecting the two stable states. A flat front solution is motionless at the Maxwell Point, where both states have the same energy [38]. For model (1), the Maxwell point corresponds to $\eta = 0$. Hence near the Maxwell point but not in this, one could expect to find a localized structure of huge size, as a consequence of the balance between front propagation and interface tension [39]. However, the equilibrium between these two effects is unstable, which corresponds to the nucleation barrier between the uniform states. In Figure 1 the nucleation barrier is represented by a dashed circle for $\eta > 0$. A circle as initial condition with radius larger (smaller) than the radius of the nucleation barrier will propagate outward (inward), as indicated by the arrows. Based on these simple energy considerations, it is straightforward to deduce that the dissipative ϕ^4 model (1) does not have stable localized structure solutions. However, introduction of spatial modulations can lead to stabilize localized structures through the front pinning effect [27]. Our goal is to show that the inclusion of spatial forcing can screening curvature effects and then give rise to new mechanisms of localized structures.

Recently, we have shown that a spatial forcing can freeze the front propagation in one-dimensional spatial system [40]. Here, in order to stop the front propagation, we consider the following two-dimensional spatially forced model

$$\partial_t u = \eta + \mu u - u^3 + \nabla^2 u + a\cos(kx) + b\cos(ky), \tag{4}$$

where $\{a, b\}$ and k are, respectively, the amplitudes and wave number of the spatial forcing. For small, and identical, forcing amplitudes ($a = b$), the uniform stable state of the dissipative forced ϕ^4 model (1) becomes a square

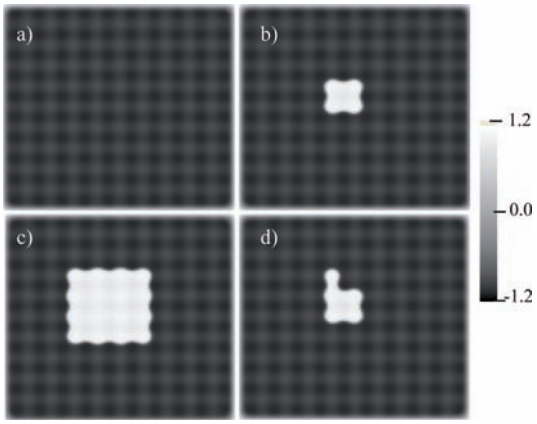

Fig. 2. Equilibrium states of the spatially forced dissipative ϕ^4 model equation (4), by $\eta = 0.01$, $\mu = 1$ and $a = 1.0$; (a) uniform state, (b), (c) and (d) localizes structures.

pattern with amplitude proportional to a (cf. Fig. 2a). Hence, in the bistability region, the above spatially forced equation is a bi-pattern system [41] with square symmetry, that is, a system that presents bistability between two spatially modulated states.

For $\eta > 0$ and small value of the amplitude a, the front propagates with a periodic speed. By increasing the amplitude a, and for a finite value, the propagative front becomes motionless and gives rise to a pinning range. This is consequence of the spatial symmetry breaking, because in order to propagate the front has to cross a periodic nucleation barrier. Hence, in the bistability region of the forced system, we observe front solutions and localized states between the two square patterns (cf. Fig. 2). As a consequence of the interplay between the envelope variations and the wave number of the underlying pattern, the front solutions are motionless in a region of parameters. Close to this region, we expect to observe a family of localized states [31,42]. In Figure 2 are shown the typical square patterns observed and the localized structures induced by the spatial forcing. As it is depicted in Figure 2, depending of the initial conditions one can observe different size and shape of the localized states.

To figure out the pinning mechanism that give rise to the localized structures, let us shed some light on the reason why a flat interface is pinned. At the Maxwell point ($\eta = 0$), the unforced model (1) has a flat motionless interface (kink solution)

$$u_k(x, y, t) = \sqrt{\varepsilon} \tanh\left[(x - P)/\sqrt{\varepsilon/2}\right],$$

where P accounts for the position of the interface. In the limit of small forcing ($a \ll 1$) and $\eta \ll 1$. This is a kink solution because this links two symmetric states [1]. We can consider the following Ansatz for the front solution

$$u(x, y, t) = \sqrt{\varepsilon} \tanh\left[(x - P(y, t))/\sqrt{\varepsilon/2}\right] + W(x, P), \quad (5)$$

where P is promoted to a field that describes the interface dynamics, and W is a small correction function. Introducing the above Ansatz in the spatially forced model

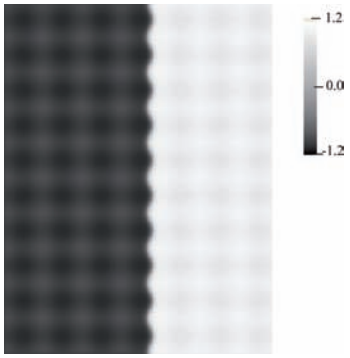

Fig. 3. Front solution of the spatially forced dissipative ϕ^4 model equation (4), by $\eta = 0.01$, $\mu = 1$ and $a = 1.0$.

equation (4), and by linearizing in W, one obtains

$$\mathcal{L}W = \eta + a\left[\cos(kx) + \cos(ky)\right] + \partial_z u_k \partial_t P + \partial_{zz} u_k \left(\partial_y P\right)^2 - \partial_z u_k \partial_{yy} P, \quad (6)$$

where $z \equiv x - P(y, t)$ is the moving coordinate and $\mathcal{L} \equiv (\varepsilon - 3u_k^2 + \partial_x^2)$ is a linear operator. Introducing the inner product $\langle f \mid g \rangle = \int_{-\infty}^{\infty} f g \, dx$, the linear operator $\mathcal{L}$ is self-adjoint ($\mathcal{L} = \mathcal{L}^\dagger$) and $\partial_z u_k$ is the only element of the kernel of $\mathcal{L}$, which is related to the Goldstone mode of the translation invariance [1]. Hence, the above equation has solution if the interface field $P(y, t)$ satisfies the following solvability condition (Fredholm alternative [1])

$$\partial_t P = -\frac{3\eta}{\sqrt{2\varepsilon}} + \gamma \cos(kP) - \frac{3a}{\sqrt{2\varepsilon}} \cos(ky) + \partial_{yy} P, \quad (7)$$

where $\gamma \equiv a \int_{-\infty}^{\infty} \partial_z u_k \cos(kz) dz / \int_{-\sqrt{\varepsilon}}^{\sqrt{\varepsilon}} \partial_z u_k du_k$. The first term on the right hand side describes the drift force related to the difference of energy between the two metastable states, the second and the third terms account for the interaction of the interface and the spatial forcing in the longitudinal, respectively, transversal direction of the interface. The last term accounts for the effects of curvature, i.e. as the speed of the front is affected by the curvature of the interface. Effects of nonlinear curvature are neglected in the scaling of validity of equation (7). It is important to note that a similar interface equation, was derived in the case of a front connecting a roll pattern with an uniform state [43].

Hence, equation (7) describes the dynamics of a flat interface between two stable solutions, which, in spatially periodic media, becomes unstable and develops a small amplitude modulation along the transverse direction, as depicted in Figure 3. This phenomenon is due to the forcing term proportional to a. The parameter $G \equiv 3\eta/\gamma\sqrt{2\varepsilon}$ stands for the balance between the drift, due to the symmetry breaking, and the periodic force induced by the spatial forcing. When G is larger than one, the front propagates along the longitudinal direction with a periodic motion. For $|G| \leq 1$, the system exhibits an infinity of equilibria that represent the different equilibrium positions of the interface. When $|G| < 1$ the interface is

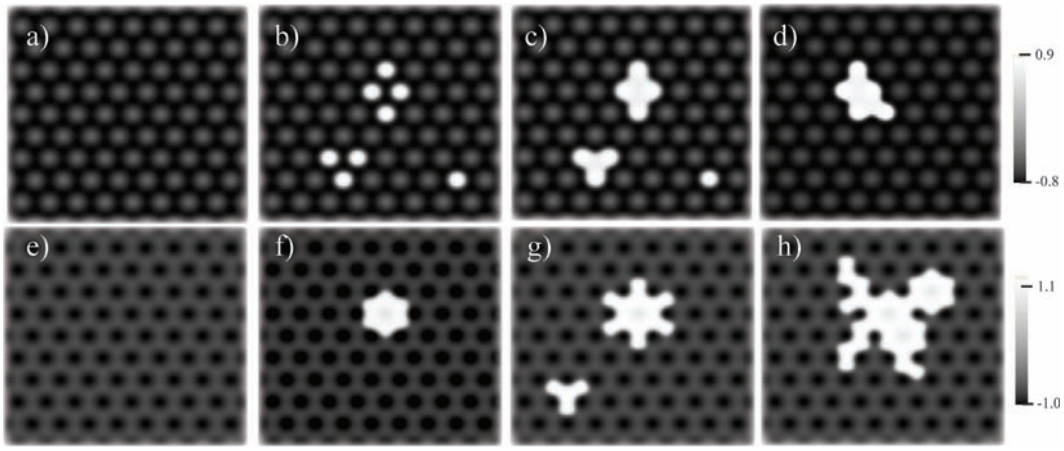

Fig. 4. Localized structures of the spatially forced dissipative ϕ^4 model equation (8) with hexagonal (upper row) and honeycomb (lower row) symmetry; (a) background state, (b), (c), (d) stable localized structures built from different initial conditions by $\eta = 0.01$, $\mu = 0.5$, and $a = b = c = 0.5$; (e) background state, (f), (g), (h) stable localized structures built from different initial conditions by $\eta = 0.01$, $\mu = 0.5$, and $a = b = -c = 0.5$.

motionless and the system exhibit a large pining range. Thus, equation (7) allows a qualitative understanding of how each piece of a localized structure is held. Furthermore, the interaction of two interfaces propagating from opposite directions can also be included in the model via a term that decreases exponentially with the distance between the interfaces. It is important to note that the previous analytical result is valid near the Maxwell and for small spatial forcing, but the mechanisms involved in this limit are qualitatively valid away from the region of validity of this result. Numerical simulations and experimental results show a good qualitative agreement.

Even though the above analysis does not provide a rigorous derivation for two-dimensional localized structures, we would like to stress that controlling and managing the pinning phenomenon, as it can be realized in spatially forced systems, constitutes a powerful qualitative approach. For example, such an approach allows us to easily construct, both numerically and experimentally, an infinite family of arbitrarily shaped localized structures, each of them resulting from the superposition or interaction between two different interfaces pinned over the spatially forced state. To illustrate the pinning phenomenon and the generation of localized states with different shapes depending on the supporting pattern, let us consider, for example, the dissipative forced ϕ^4 model with an hexagonal type forcing

$$\partial_t u = \eta + \mu u - u^3 + \nabla^2 u + a\cos(kx) + b\cos\left(k\frac{x-\sqrt{3}y}{2}\right) + c\cos\left(k\frac{x+\sqrt{3}y}{2}\right), \quad (8)$$

where $\{a, b, c\}$ and k are the amplitudes and wave number of the spatial forcing. For small identical forcing amplitudes ($a = b = c$) or anti-symmetrical ones ($b = c = -a$), the uniform stable state becomes an hexagonal or, respectively, honeycomb pattern with amplitude proportional to a. Hence, in the bistability region, the above spatially forced equation is a bi-pattern system with hexagonal symmetry.

In Figure 4 are shown the typical hexagonal patterns observed and the interfaces between them. As in the case of the square forcing, we expect, also in the hexagonally forced system, a family of localized structures to result as a consequence of the pinning phenomenon. Indeed, by changing the initial conditions, we observe different stable localized states. A few examples of them are shown in Figure 4. To summarize, the spatial forcing allows us to stabilize and to create a family of arbitrarily shaped-localized structures, where the size and the shape of the interface is led by the form of the spatial forcing. Note that pinning of localized structures on periodic arrays has also been reported for a fixed grid in asymmetric vortex [44]. We note that if one considers a sufficiently large amplitude forcing the curvature effects are negligible. Therefore the dynamics of the interface is dominated by typical effects of one-dimensional systems.

3 Experimental set-up

The experimental set-up used for the generation of localized structures in two-dimensional spatially periodic media is a LCLV with optical feedback. A schematic picture of the experiment is given in Figure 5.

The LCLV with optical feedback is a system characterized by very rich dynamics, enabling the observation of different types of spatial structures and symmetries depending on the various experimental configurations [45]. In the present experiment, we fix bistability between different homogenous states, which is realized by introducing polarization interference and zero length of diffraction in the feedback loop [46]. Moreover, we introduce the spatial forcing by using a spatial light modulator SLM, able to produce both phase and amplitude modulations on the input beam profile [47].

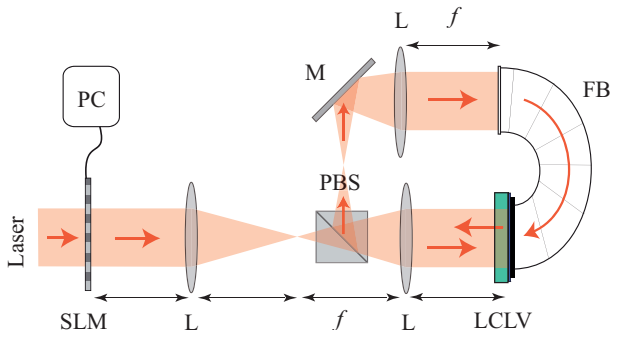

Fig. 5. (Color online) Schematic experimental set-up. L are lenses of the same focal length, $f = 250$ mm; PBS polarizing beam-splitter; SLM spatial light modulator; PC personal computer; M mirror; FB fiber bundle.

The LCLV consists of a thin film of a nematic liquid crystal, LC, interposed between a glass plate and a photoconductive material on which a dielectric mirror is deposed. The inner surfaces of the cell are prepared for planar anchoring of the liquid crystals (nematic director parallel to the confining walls) [48]. Thanks to transparent electrodes, a voltage can be applied across the LC layer and all the molecules tend to orient along the same average direction defined by the applied electric field. When a light beam impinges on the photoconductive side of the valve, because of the photo-induced charges the effective voltage across the LC layer increases, leading to a further reorientation of the liquid crystal molecules. Because of the LC birefringence, the molecular reorientation produces a refractive index change for the beam passing through the LC layer, hence a phase variation, and the LCLV as a whole acts as a Kerr like medium, providing for the reflected beam a phase shift $\varphi = kdn_2 I_w$ proportional to the "write" intensity I_w incident onto the photoconductor. Here k is the optical wave number, d the thickness of the nematic layer and $n_2 = n_2(V_0)$ the equivalent non linear coefficient of the LCLV.

The LCLV is illuminated by an expanded He-Ne laser beam ($\lambda = 632.8$ nm), 3 cm transverse diameter, linearly polarized along the vertical direction. Once shone onto the LCLV, the beam is reflected back by the dielectric mirror deposed on the rear side of the cell and, thus, sent in the feedback loop. A polarizing beam-splitter, PBS, a mirror, M, and an optical fiber bundle, FB, are used to close the loop and to send the beam back to the photoconductive side of the LCLV. The liquid crystal director is oriented at 45°. The PBS introduces polarization interference between the ordinary and extraordinary waves propagating in the loop, thus providing bistability between differently orientated states of the liquid crystal molecules [45]. This, together with the diffraction-free situation, are the main ingredients necessary to get bistability between homogeneous states, hence, *normal fronts* connecting spatially uniform extended states [46]. These fronts correspond to different average orientations of the liquid crystal molecules and appear in the transverse direction of the beam propagation as moving interfaces between different levels of the light intensity.

In the feedback loop, a self-imaging configuration is obtained by using two lenses of the same $f = 25$ cm focal length, placed in such a way that the rear side and the front side of the LCLV are conjugate planes. A spatial light modulator, SLM, is placed on the optical path of the input beam and a third lens of the same $f = 25$ cm focal length, provides a 1:1 imaging of the SLM onto the front side of the LCLV. The SLM is a liquid crystal display, one inch diagonal size, with a 1024×768 pixels, each coded in 8 bits of intensity level, interfaced with a personal computer, PC. By using a dedicated software, intensity masks are produced and sent to the SLM, which acts as a programmable filter able to impose arbitrary spatial modulations on the input beam profile. Two-dimensional intensity forcings are introduced in order to generate and control localized structures of different symmetry and size.

3.1 Theoretical description of the spatial forcing in the LCLV with optical feedback

The model describing the evolution of the average orientation angle θ of the liquid-crystal molecules, as originally developed in [36], consists in a diffusive and relaxation equation for the average liquid crystal tilt angle $\theta(x,t)$, $0 \leq \theta \leq \pi/2$, coupled with an equation for the feedback light intensity I_w [45]. In the case of zero diffraction length in the feedback loop, the equation for I_w can easily be solved, and the full model for the LCLV with optical feedback reads as

$$\tau \partial_t \theta = l^2 \nabla_\perp^2 \theta - \theta + \begin{cases} 0, & V_{LC} < V_{FT} \\ \frac{\pi}{2}\left(1 - \sqrt{\frac{V_{FT}}{V_{LC}(\theta)}}\right), & V_{LC} \geq V_{FT} \end{cases} \tag{9}$$

where $\tau = 30$ ms is the liquid cristal relaxation time, $l = 30$ μm the electric coherence length, $\nabla_\perp^2$ the transverse Laplacian and $V_{LC}(\theta) \equiv \Gamma V_0 + \alpha I_w$ the effective voltage applied to the liquid crystals, with $V_{FT} = 3.2\, V_{rms}$ the threshold for the Fréedericksz transition, $\Gamma \sim 0.3$ the overall impedance of the LCLV dielectric layers and $\alpha \sim 5.5$ V cm^2/mW a phenomenological parameter summarizing, in the linear approximation, the response of the photoconductor. The light intensity reaching the photoconductor is $I_w = I_{in}[1 - \cos(\Delta\varphi)]$, where $\Delta\varphi = \beta \cos^2\theta$ is the overall phase shift experienced by the light traversing the LC layer, $\beta = 2kd\Delta n$ with $d = 15$ μm the thickness of the nematic layer, $\Delta n = 0.2$ the LC birefringence and $k = 2\pi/\lambda$ with $\lambda = 632.8$ nm.

Close to the point of nascent bistability, $I_{in} \equiv I_c$, $V_0 \equiv V_c$ and $\theta \equiv \theta_0$, and considering a spatially modulated intensity $I_{in} = I_c + B[\cos(2\pi x/p) + \cos(2\pi x/p)]$, we can reduce the full θ model to a forced dissipative ϕ^4-model that reads as

$$\tau \partial_t \phi = \eta + \mu\phi - \phi^3 + l^2 \nabla_\perp^2 \phi + a\left[\cos\left(\frac{2\pi x}{p}\right) + \cos\left(\frac{2\pi y}{p}\right)\right], \tag{10}$$

where p is the wavelength of the spatial modulation and ϕ is the order parameter, which is related to the average

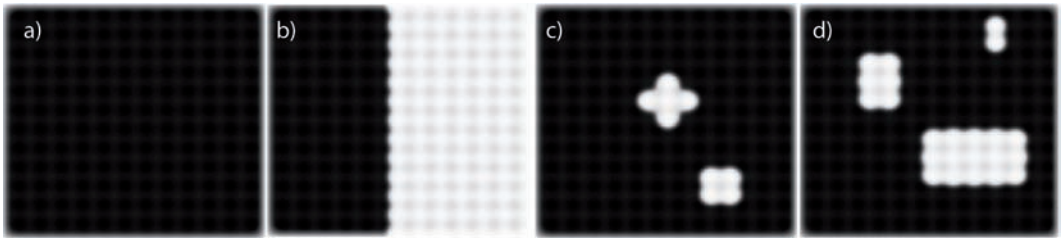

Fig. 6. Numerical simulations of the average liquid crystal tilt angle model equation (9) by $V_{FT} = 3.2$, $I_c = 0.75$, $\beta = 59$, $a = 0.1$ and $p = 0.8$; (a) background state, (b) front between the background and the upper state, (c) and (d) examples of stable localized structures.

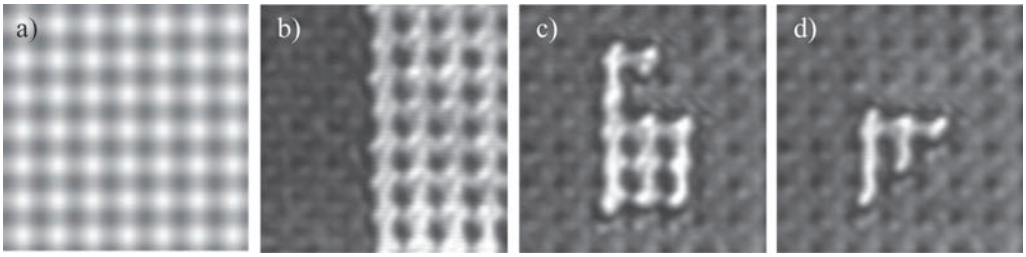

Fig. 7. Localized structures observed in the experiment for a square grid modulation of the input beam; $A = 190$, $B = 30$, $p = 150$ μm: (a) intensity mask delivered by the SLM; (b) front between the background and the upper state, $V_0 = 5.6$ V; (c) and (d) examples of localized structures, (c) $V_0 = 5.4$ V and (d) $V_0 = 5.3$ V.

director tilt by the expression

$$\theta \approx \theta_0 + \phi / \Big(2\beta \cos 2\theta_0 \cot\left(\beta \cos^2 \theta_0\right) + \left(4 + \beta^2 \sin 2\theta_0\right)/3 - 2/\left(\pi/2 - \theta_0\right)^2 \Big)^{1/2}.$$

The various coefficient η, ϵ, b and c can be calculated with respect to the different experimental parameters and read as

$$\eta \equiv \frac{2\alpha}{\pi^2 V_{FT}} \left[1 - \cos\left(\beta \cos^2 \theta_0\right)\right] \left(\pi/2 - \theta_0\right)^3 \times \left[\Gamma I_{in} - \Gamma I_c + \alpha \left(1 - \cos\left(\beta \cos^2 \theta_0\right) \left(V_0 - V_c\right)\right)\right],$$

$$\mu \equiv \frac{12}{\pi^2 V_{FT}} \left[\left(\pi/2 - \theta_0\right)^2 \left(V_0 - V_c\right)\right] + \frac{12}{\pi^2 V_{FT}} \times \left[\left(\frac{\pi^2 V_{FT}}{12} - \left(\pi/2 - \theta_0\right)^2\right) \left(I_{in} - I_c\right)/I_c\right],$$

$$a \equiv \frac{2\alpha B}{\pi^2 \Gamma V_{FT}} \left[1 - \cos\left(\beta \cos^2 \theta_0\right)\right] \left(\pi/2 - \theta_0\right)^3.$$

Numerical simulations of the full LCLV model equation (9) exhibit qualitatively the same types of localized structures shown by the dissipative forced ϕ^4 model. In Figure 6 are depicted the typical background state, the front solution between this state and the upper state, and a few examples of localized structures obtained from the integration of equation (9).

4 Experimental results

To confront theoretical results with experiments, two dimensional spatial modulations have been imposed in the LCLV system by suitable intensity profiles of the input beam. At this purpose, starting from fronts connecting two homogeneous states, appropriate spatial modulations have been introduced on the input beam profile via the SLM, as described in the previous section. Both square and hexagonal grids have been used to produce fronts in two-dimensional spatially modulated media as well as to generate and control localized structures in the range of parameters where fronts can be pinned.

Let us first consider localized states over a square grid. Suitable intensity distributions are generated through the SLM, so that the input intensity takes the following expression,

$$I(x, y) = A + B\left[\cos\left(k\,x\right) + \cos\left(k\,y\right)\right],$$

with x the horizontal direction, y the vertical one and $k = 2\pi/p$, where p is the wavelength of the modulation. Here the intensity is expressed in gray levels, from 0 and 255, as delivered by the SLM. For an uniform mask of 185 gray value the input intensity is $I_{in} = 0.84$ μW/cm^2. A typical square intensity mask is displayed in Figure 7a, for grid parameters $A = 190$, $B = 30$ and $p = 150$ μm. In Figure 7b is shown an interface between the square modulated background and the upper state observed in the pinning range of the front, $V_0 = 5.6$ V, whereas Figure 7c and 7d display examples of stable localized structures obtained for $V_0 = 5.4$ V and $V_0 = 5.3$ V, respectively, and same forcing parameters.

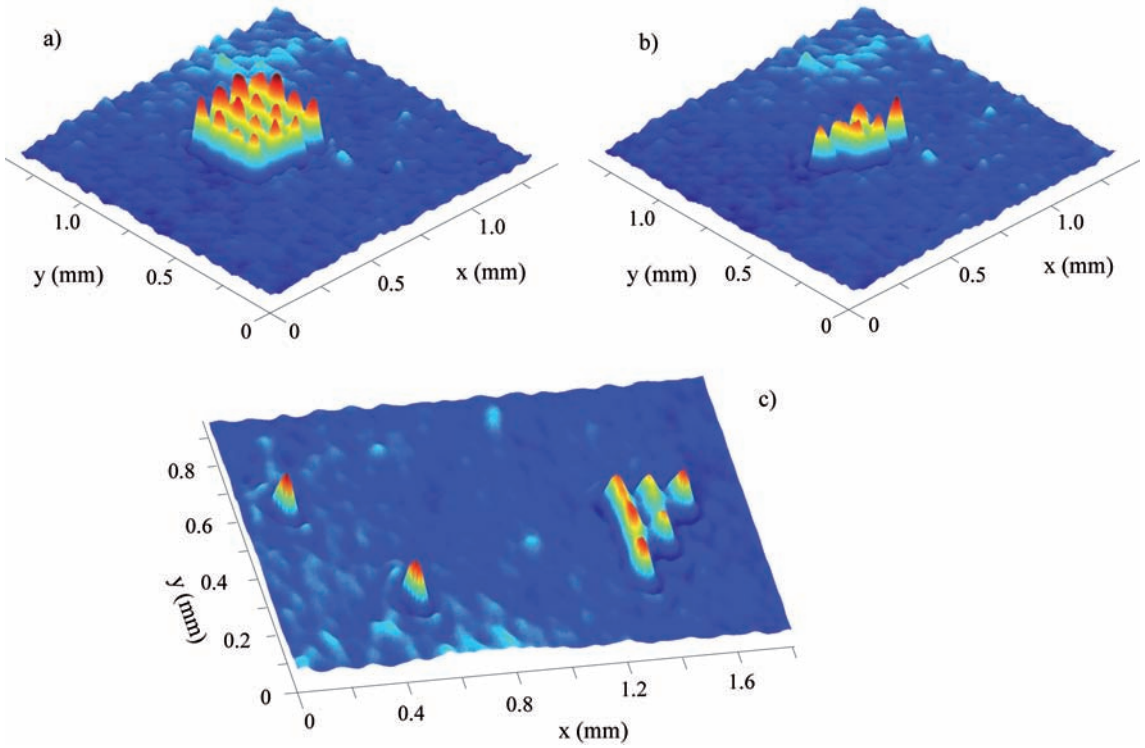

Fig. 8. (Color online) Localized structures experimentally observed over a square grid for different initial conditions: (a) square shaped localized domain comprising 16 cells of the underlying grid; (b) 6 cells localized structure obtained from selective erasing individual cells of the large square domain; (c) "F" shaped localized domain and two single-cell localized structures. Experimental parameters are $V_0 = 5.7$ V, $A = 180$, $B = 15$ and $p = 100$ μm.

Then, in order to put into evidence the control and managing of two-dimensional localized structures of arbitrary shape through the pinning phenomenon, we have proceeded in the following way. By using the SLM, a square shaped initial condition of 255 gray level over a square grid background is switched on and then off, for a fixed voltage V_0 inside the pinning range. Figure 8a shows the stable localized square domain obtained and having the same size of the initial condition. This localized state consists of 16 cells of the underlying square grid. By using the cursor of the computer driving the SLM, it is possible to apply locally a small perturbation that, because of the bistable behavior of the system, allows us to selectively erase individual cells of the localized domain. With this procedure, we can stabilize localized structures of different shapes. As an example, in Figure 8b it is shown a localized domain comprising 6 cells of the underlying square grid. For the same experimental parameters another example of localized states is displayed by Figure 8c, where one can distinguish a structure having the shape of a "F" letter as well as two single-cell localized structures.

It is worth noting that for a given voltage V_0 in the left part in the pinning range, there is a maximum size for the domain that one can stabilize. Starting from this maximum domain size, smaller ones can be stabilized by applying the erasing process previously described. When increasing V_0, thus approaching the right border of the pinning range, one tends to deal with domains more difficult to stabilize as the system is getting nearer to the depinning transition, and so closer to the upper front solution [40]. Moreover, if instead of using a localized initial condition one uses an extended one, it is possible to get extended modulated front, as displayed in Figure 9a. By displacing the cursor on the intensity mask we can perform a selective erasing of the pattern cells and get a new state as depicted in Figure 9b.

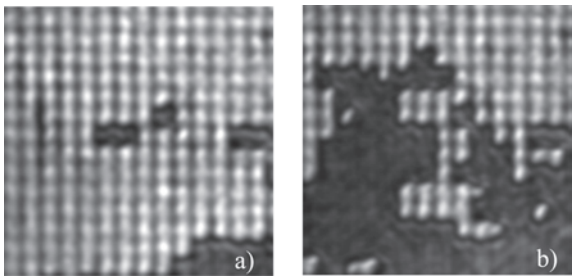

Fig. 9. Fronts over a square grid; (a) initial state, (b) new state resulting from selective erasing of the pattern cells. Experimental parameters are $V_0 = 5.8$ V, $A = 180$, $B = 15$, $p = 100$ μm.

We can proceed in a similar way by replacing the square modulation with an hexagonal grid and, thus, generate localized states over an hexagonally modulated medium. Suitable intensity profiles of the input beam were

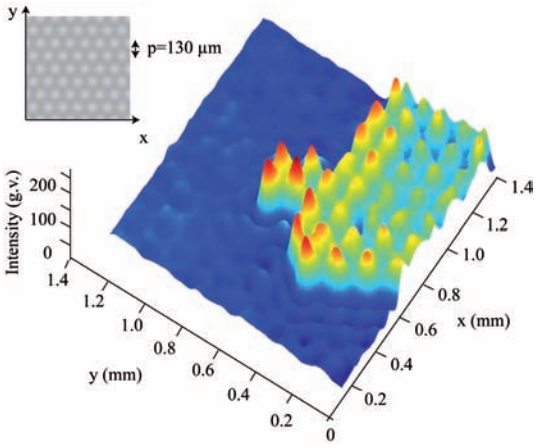

Fig. 10. (Color online) Front between the two hexagonally modulated states for $V_0 = 5.8$ V and modulation parameters $A = 187.5$, $B = 7.5$, $p = 130$ μm. In the inset it is shown the corresponding hexagonal mask displayed on the SLM.

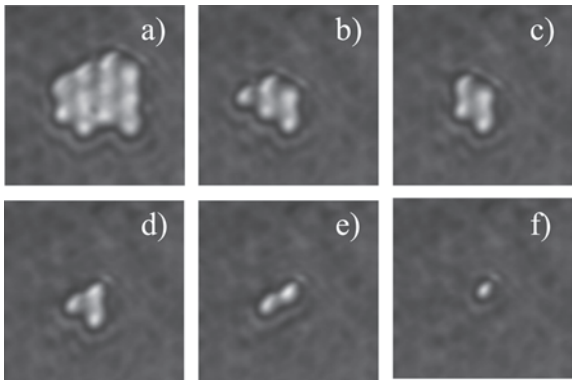

Fig. 11. Localized states over an hexagonally modulated medium for $V_0 = 5.8$ V and modulation parameters $A = 187.5$, $B = 7.5$, $p = 130$ μm; (a) 11 cells, (b) 5 cells, (c) 4 cells, (d) 3 cells, (e) 2 cells and (d) single-cell localized structure.

produced in the form

$$I(x,y) = A + B\left[\cos(k\,x) + \cos\left(\frac{1}{2}k\,x + \frac{\sqrt{3}}{2}k\,y\right)\right] + B\left[\cos\left(\frac{1}{2}k\,x - \frac{\sqrt{3}}{2}k\,y\right)\right],$$

with $k = 2\pi/p$. A front between an hexagonal grid background and the corresponding upper state is shown in Figure 10 for $V_0 = 5.8$ V and forcing parameters $A = 187.5$, $B = 7.5$, $p = 130$ μm, with $I_{in} = 0.84$ μW/cm^2 for an uniform mask of 185 gray value.

For the same applied voltage $V_0 = 5.8$ V, and for the same forcing parameters as above, different localized states can be stabilized starting from appropriate initial conditions. As shown in Figure 11, we observe localized structures with different size, going from 1 to 11 cells of the underlying hexagonal grid. To produce them, we start from a stable domain generated starting from a circular initial condition and, by using the SLM, we apply the same erasing process as described above for the square grid. This way, it is possible to selectively erase the peripheric cells of the stable domain and to stabilize smaller states, down to a single-cell localized structures, as depicted in Figure 11.

A generalization of the above description can be made by considering intensity masks with more complex symmetry, like quasi-crystal patterns or super-lattices. This could be implemented by using a generalized formula

$$I(x,y) = A + B\Sigma_i\left[\cos\left(\boldsymbol{k_i}\cdot\boldsymbol{r}\right)\right],$$

with $\boldsymbol{r} = (x,y)$ and $\Sigma_i \boldsymbol{k_i} = \boldsymbol{0}$. Localized structures with complex symmetries are expected to arise in such systems and further investigations in this direction are in progress.

5 Conclusions

We have shown that an optical system characterized by a robust bistability range between homogeneous or uniform states allows achieving a high level of control and managing of localized structures by means of a two-dimensional spatial forcing. By using an experimental set-up based on a liquid crystal cell with optical feedback, we have shown that it is possible to stabilize a large set of localized structures with arbitrary shape and size and that these features are controlled by the symmetry and wavelength of the underlying grid. The control of the localized states is ensured by the mastering of the forcing grid and of its constitutive parameters. The protocol of writing and erasing the different localized structures has been proved over a square and an hexagonal grid and has been shown to be robust and reproducible. Numerical simulations of the full model for the LCLV with optical feedback confirm the experimental findings.

Close to the points of nascent bistability, we have introduce a dissipative ϕ^4 model as a prototype for spatially bistable forced systems, and we have shown that with different spatial forcings, such as square or hexagonal grids, this model exhibits a family of localized structures. The approach is very general and extension of the same protocol to other experimental systems is straightforward. By introducing spatial modulations with different symmetries more complex localized structures could be observed and exploited for more complicated tasks of optical storage and processing.

M.G.C. acknowledges the FONDECYT project 1090045. R.G.R. thanks the FONDECYT project 11080286. U.B. and S.R. thanks the ANR-07-BLAN-0246-03, *turbonde*.

References

1. See, e.g., L.M. Pismen, *Patterns and Interfaces in Dissipative Dynamics* (Springer Series in Synergetics, Berlin, Heidelberg, 2006), and references therein
2. R.A. Fisher, Ann. Eugenics **7**, 335 (1937)
3. A. Kolmogorov, I. Petrovsky, Piskunov, Bull. Univ. Moskou Ser. Int. Se. **7**, 1 (1937)
4. J.D. Murray, *Mathematical Biology* (Springer-Verlag, Berlin, 1993)
5. P. Kife, *Mathematical Aspects of Reacting and Diffusing System*, edited by S. Levin, Lecture Notes in Biomathematics **28** (Springer-Verlag, New York, 1979)
6. D. Walgraef, *Spatio-temporal pattern formation* (Springer-Verlag, New York, 1997)
7. G. Dee, J.S. Langer, Phys. Rev. Lett. **50**, 383 (1983)
8. P. Manneville, *Dissipative structures and weak turbulence* (Academic Press, San Diego, 1990)
9. D.G. Aronson, H.F. Weinberger, Adv. Math. **30**, 33 (1978)
10. P. Collet, J.P. Eckmann, *Instabilities and fronts in extended system* (Princeton University Press, New Jersey, 1990)
11. M. Cross, P. Hohenberg, Rev. Mod. Phys. **65**, 851 (1993)
12. H.A. Eschenfelder, *Magnetic Bubble Technology* (Springer Verlag, Berlin, 1981)
13. S. Pirkl, P. Ribière, P. Oswald, Liq. Cryst. **13**, 413 (1993)
14. Y.A Astrov, Y.A. Logvin, Phys. Rev. Lett. **79**, 2983 (1997)
15. K.-J. Lee, W.D. McCormick, J.E. Pearson, H.L. Swinney, Nature **369**, 215 (1994)
16. W.S. Edwards, S. Fauve, J. Fluid Mech. **278**, 123 (1994)
17. P.B. Umbanhowar, F. Melo, H.L. Swinney, Nature **382**, 793 (1996)
18. M.G. Clerc, P. Cordero, J. Dunstan, K. Huff, N. Mujica, D. Risso, G. Varas, Nat. Phys. **4**, 249 (2008)
19. R. Heinrichs, G. Ahlers, D.S. Cannell, Phys. Rev. A **35**, 2761(R) (1987)
20. P. Kolodner, D. Bensimon, C.M. Surko, Phys. Rev. Lett. **60**, 1723 (1988)
21. D.W. Mc Laughlin, J.V. Moloney, A.C. Newell, Phys. Rev. Lett. **51**, 75 (1983)
22. N.N. Rosanov, G.V. Khodova, Opt. Spectrosc. **65**, 449 (1988)
23. T. Ackemann, W.J. Firth, G.L. Oppo, Adv. At. Mol. Opt. Phys. **57**, 323 (2009)
24. W. van Saarloos, P.C. Hohenberg, Phys. Rev. Lett. **64**, 749 (1990)
25. P.D. Woods, A.R. Champneys, Physica D **129**, 147 (1999)
26. G.W. Hunt, G.J. Lord, A.R. Champneys, Comput. Meth. Appl. Mech. Eng. **170**, 239 (1999)
27. Y. Pomeau, Physica D **23**, 3 (1986)
28. P. Coullet, C. Riera, C. Tresser, Phys. Rev. Lett. **84**, 3069 (2000)
29. J. Burke, E. Knobloch, Phys. Rev. E **73**, 056211 (2006)
30. J. Burke, E. Knobloch, Chaos **17**, 037102 (2007)
31. M.G. Clerc, C. Falcon, Physica A **356**, 48 (2005)
32. U. Bortolozzo, M.G. Clerc, C. Falcon, S. Residori, R. Rojas, Phys. Rev. Lett. **96**, 214501 (2006)
33. W.J. Firth, L. Columbo, A.J. Scroggie, Phys. Rev. Lett. **99**, 104503 (2007)
34. U. Bortolozzo, M.G. Clerc, S. Residori, Phys. Rev. E **78**, 036214 (2008)
35. U. Bortolozzo, M.G. Clerc, S. Residori, New J. Phys. **11**, 093037 (2009)
36. M.G. Clerc, A. Petrossian, S. Residori, Phys. Rev. E **71**, 015205(R) (2005)
37. S.H. Strogatz, *Nonlinear Dynamics and Chaos: With Applications to Physics, Biology, Chemistry and Engineering* (Addison-Wesley, Reading, Massachussets, 1994)
38. R.E. Goldstein, G.H. Gunaratne, L. Gil, P. Coullet, Phys. Rev. A **43**, 6700 (1991)
39. P. Coullet, Int. J. Bifur. Chaos **12**, 2445 (2002)
40. F. Haudin, R.G. Elías, R.G. Rojas, U. Bortolozzo, M.G. Clerc, S. Residori, Phys. Rev. Lett. **103**, 128003 (2009)
41. U. Bortolozzo, M.G. Clerc, F. Haudin, R.G. Rojas, S. Residori, Adv. Nonlinear Opt. **2009**, 926810 (2009)
42. D. Bensimon, B.I. Shraiman, V. Croquette, Phys. Rev. A **38**, R5461 (1988)
43. M.G. Clerc, D. Escaff, C. Falcon, E. Tirapegui, Eur. Phys. J. Special Topics **143**, 171 (2007)
44. T.J. Alexander, A.A. Sukhorukov, Y.S. Kivshar, Phys. Rev. Lett. **93**, 063901 (2004)
45. S. Residori, Phys. Rep. **416**, 201 (2005)
46. M.G. Clerc, S. Residori, C.S. Riera, Phys. Rev. E **63**, 060701(R) (2001)
47. U. Bortolozzo, S. Residori, Phys. Rev. Lett. **96**, 037801 (2006)
48. P.G. De Gennes, J. Prost, *The Physics of Liquid Crystals*, second edition (Oxford Science Publications, Clarendon Press, 1993)